RSC Advances

PAPER

View Article Online
View Journal | View Issue

Cite this: *RSC Adv.*, 2024, **14**, 27873

Copper-doped cherry blossom carbon dots with peroxidase-like activity for antibacterial applications†

Yitong Wang,[a] Tianliang Li,[b] Lixing Lin,[b] Dong Wang[b] and Lingyan Feng *[abc]

Safety concerns arising from bacteria present a significant threat to human health, underscoring the pressing need for the exploration of novel antimicrobial materials. Nanozymes, as a new type of nanoscale material, have attracted widespread attention for antibacterial applications owing to their ability to mimic the catalytic activity of natural enzymes. In this work, we have constructed copper-doped cherry blossom carbon dots (Cu-CDs) with excellent peroxidase-like (POD) activity using a one-pot hydrothermal method. The utilization of cherry blossom as a natural material precursor significantly enhances its biocompatibility. Furthermore, the incorporation of copper ions initiates Fenton-like reaction-triggered POD-like catalytic activity, effectively eradicating bacteria by converting hydrogen peroxide (H_2O_2) into hydroxyl radicals (·OH). The antibacterial test results demonstrate that Cu-CDs exhibit a bactericidal efficacy of over 90% against *Escherichia coli* (*E. coli*) and *Staphylococcus aureus* (*S. aureus*). This study presents a novel environmentally friendly nanozyme material derived from natural sources, exhibiting significant antimicrobial properties and offering innovative insights for the advancement of antimicrobial materials.

Received 24th June 2024
Accepted 29th August 2024

DOI: 10.1039/d4ra04614e

rsc.li/rsc-advances

1. Introduction

Bacterial infections pose a formidable challenge to global public health, and are capable of causing a range of diseases such as tuberculosis, pneumonia, sepsis, and meningitis.[1–4] Currently, the use of antibiotics is still a highly effective means for treating bacterial diseases.[5] However, the search for safer and more potent alternatives is ongoing, with a focus on materials that can provide exceptional antimicrobial performance (Scheme 1).

Nanozymes, as functional nanomaterials with enzymatic-like activities, have demonstrated the potential to overcome the inherent drawbacks of natural enzymes, such as poor stability, high sensitivity to environmental conditions, and exorbitant production costs.[6] Consequently, the design of functional nanomaterials with enzymatic catalytic activity as stable and cost-effective substitutes for natural enzymes has garnered significant interest among scientists.[7] In recent years, various nanomaterials, including metal nanoparticles, metal oxide nanoparticles, and carbon-based nanomaterials (such as carbon dots (CDs), graphite, graphene, and graphene oxide), have been reported to exhibit peroxidase (POD)-like activity and have shown potential applications in biomedical applications, environmental monitoring, and bionics.[8–10] Notably, POD-like nanozymes that catalyse hydrogen peroxide H_2O_2 into highly reactive oxygen species (ROS), especially hydroxyl radicals (·OH), have attracted attention.[11] The generated ROS can attack bacterial cell membranes, leading to bacterial death and thereby achieving bactericidal effects.[12]

With the rapid development of nanotechnology, CDs have become a hot topic of research due to their unique

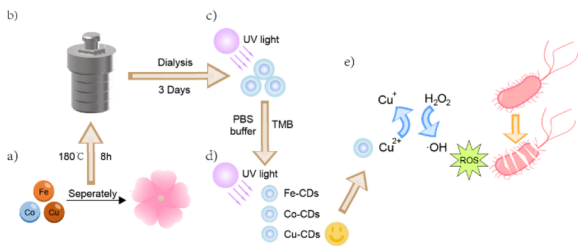

Scheme 1 Synthesis and application of CDs. (a) Doping of three different metal elements into cherry blossoms to synthesize metal-doped CDs. (b) A one-step hydrothermal process is employed for the synthesis. (c) The resulting CDs exhibit bright blue fluorescence. (d) The catalytic activity of these CDs, analogous to POD, is assessed. (e) Specifically, Cu-CDs demonstrate exceptional antibacterial properties.

[a]QianWeichang College, Shanghai University, Shanghai 200444, China. E-mail: lingyanfeng@t.shu.edu.cn

[b]Materials Genome Institute, Shanghai Engineering Research Center for Integrated Circuits and Advanced Display Materials, Shanghai Engineering Research Center of Organ Repair, Shanghai University, Shanghai 200444, China

[c]Joint International Research Laboratory of Biomaterials and Biotechnology in Organ Repair, Ministry of Education, Shanghai 200444, China

† Electronic supplementary information (ESI) available. See DOI: https://doi.org/10.1039/d4ra04614e

physicochemical properties and biocompatibility.[13] CDs are a class of nanoscale carbon-based materials, typically with a spherical structure less than 10 nm in diameter.[14] Compared to traditional materials, CDs offer advantages such as low toxicity and good biocompatibility, attributed to their carbon core structure, which makes them less likely to provoke immune responses or inflammation within biological systems.[15–18] In addition, with the ease of modification, CDs demonstrate immense potential in applications such as biomedicine, energy catalysis, and optoelectronics.[19,20]

Scientists frequently utilize plants as a carbon source to synthesize CDs with POD-like activity and explore their applications. For instance, Du *et al.*[21] prepared silicon-doped CDs (Si-CDs) from peanut shells through a one-pot hydrothermal process. These CDs exhibit POD-like activity and can be applied to detect the level of cysteine (Cys) in food. In addition, Zhu *et al.*[22] synthesized iron-doped carbon quantum dots (Fe-CQDs) from waste coffee grounds using a simple hydrothermal method. These CQDs demonstrate high POD-like activity and can be used for colorimetric and fluorescent detection of ascorbic acid (AA). In this study, we selected cherry blossoms as the carbon source for their availability and symbolic status as a spring icon in Japan.[23,24] This choice also aligns with the widespread cultivation of cherry blossoms in Shanghai. In prior researches, it has been observed that the extracts from cherry blossoms are believed to have anti-inflammatory and anti-aging effects.[25–27] Additionally, Huang *et al.*[28] reported the synthesis of CDs from cherry blossoms, proposing potential applications in fluorescent ink, metal ion sensors, and cell imaging agents. However, their study did not investigate the POD-like activity of these CDs. By synthesizing CDs with cherry blossoms as a carbon source and examining their POD-like activity, our research not only delves into a novel application but also underscores the benefits of harnessing naturally occurring, eco-friendly materials. In contrast to conventional POD-mimetic CDs that are typically synthesized using chemical reagents, this approach aligns with the principles of green chemistry and could pave the way for sustainable production of POD-mimetic CDs.[29,30]

Expanding on the existing body of research, our observations indicate that the strategic doping of carbon dots with metal or nonmetal elements, such as manganese (Mn), iron (Fe), copper (Cu), selenium (Se), and others, can markedly improve their chemical characteristics. This enhancement, in turn, leads to a notable increase in the efficacy of the nanozymes.[31–35] In this work, we modified them by doping with metal elements.[36] We doped the initial CDs with three metal elements, Fe, cobalt (Co), and Cu, which have been previously reported to significantly enhance the POD-like activity of the material to prepare iron-doped carbon dots (Fe-CDs), cobalt-doped carbon dots (Co-CDs) and copper-doped carbon dots (Cu-CDs).[37–40] Among the three metal-doped CDs, Cu-CDs demonstrated the most outstanding POD-like activity. The Cu-CDs possess catalytic properties that enable them to decompose hydrogen peroxide efficiently, resulting in the formation of potent hydroxyl radicals (·OH). These radicals are crucial in antimicrobial applications due to their ability to exert strong oxidative effects against microbes.[41–43] Due to their high catalytic efficiency, Cu-CDs excel at disrupting bacterial cell walls and membranes and inhibiting bacterial growth, thus showing great potential in antimicrobial therapy.[44] These findings not only provide a new direction for the further study and development of nanozymes but also offer valuable insights for scientists and engineers in related fields, promoting the application and development of nanomaterials in areas such as biomedicine.

2. Results and discussion

2.1 Preparation and characterization of the CDs nanozymes

In this study, we successfully synthesized the desired Fe-CDs, Co-CDs, and Cu-CDs nanozymes using $FeCl_3 \cdot 6H_2O$, $CoCl_2 \cdot 6H_2O$ and $CuCl_2 \cdot 2H_2O$, and cherry blossom powder as precursor reactants through a simple one-pot hydrothermal method. Morphological characterization and fluorescence studies confirmed the successful synthesis of CDs, Fe-CDs, Co-CDs, and Cu-CDs. Analysis of transmission electron microscopy (TEM) images (Fig. 1a) revealed that Cu-CDs and other three CDs (Fig. S1, ESI†) exhibited a uniform spherical shape with good dispersity, and a size within the range of 10 nm. Additionally, in the high-resolution transmission electron microscopy (HR-TEM) image of non-doped CDs (Fig. S1, ESI†), a clear crystalline structure of the product was observed, with a lattice spacing corresponding to the (100) plane of graphite carbon at 0.23 nm.

The composition and chemical bonding state of the prepared CDs were characterized by Fourier-transform infrared (FT-IR) spectroscopy (Fig. 1b). The absorption peaks at 3440 cm^{-1}, 2910 cm^{-1}, 2850 cm^{-1}, 1790 cm^{-1}, 1620 cm^{-1}, and 1380 cm^{-1} were attributed to O–H/N–H, C–H, CH_2, C=O, C=C, and C–N groups.[28] For Fe-CDs, Co-CDs, and Cu-CDs, the peaks at 592 cm^{-1}, 576 cm^{-1}, and 527 cm^{-1} were attributed to Fe–O, Co–N, and Cu–O groups, respectively.[45–47] These results indicate the presence of nitrogen-containing groups (pyridinic N, pyrrolic N, and alkyl amine) and oxygen-containing groups (hydroxyl and carboxyl), providing preliminary evidence of successful metal doping within the CDs.

X-ray photoelectron spectroscopy (XPS) revealed peaks for C 1s, N 1s, and O 1s elements at 285.08 eV, 398.08 eV, and 532.08 eV in Cu-CDs (Fig. 1c) and other three CDs (Fig. S2, ESI†). The high-resolution XPS spectra for the C 1s, N 1s, and O 1s regions of all CDs are depicted in Fig. S3, ESI.† For the Cu-CDs, the C 1s spectrum displays three distinct peaks at 284.44 eV, 286.01 eV, and 287.95 eV, corresponding to the C–C/C=C, C–O, and C=O bonding environments, respectively. The N 1s spectrum of the Cu-CDs presents two peaks at 399.64 eV and 399.81 eV, which are indicative of the presence of N–C and N–H groups. Similarly, the O 1s spectrum of the Cu-CDs is characterized by three peaks at 531.06 eV, 532.87 eV, and 531.96 eV, attributed to the C=O, C–O, and O=C–O (carbonyl in an ester group) functionalities, respectively. And the other CDs also exhibit peaks at adjacent positions, indicating they possess the same functional groups. Furthermore, absorption peaks for Fe-CDs, Co-CDs, and Cu-CDs were observed at 707.19 eV, 782.30 eV, and 933.91 eV, respectively, which, consistent with the FT-IR analysis, confirmed the successful doping of metal

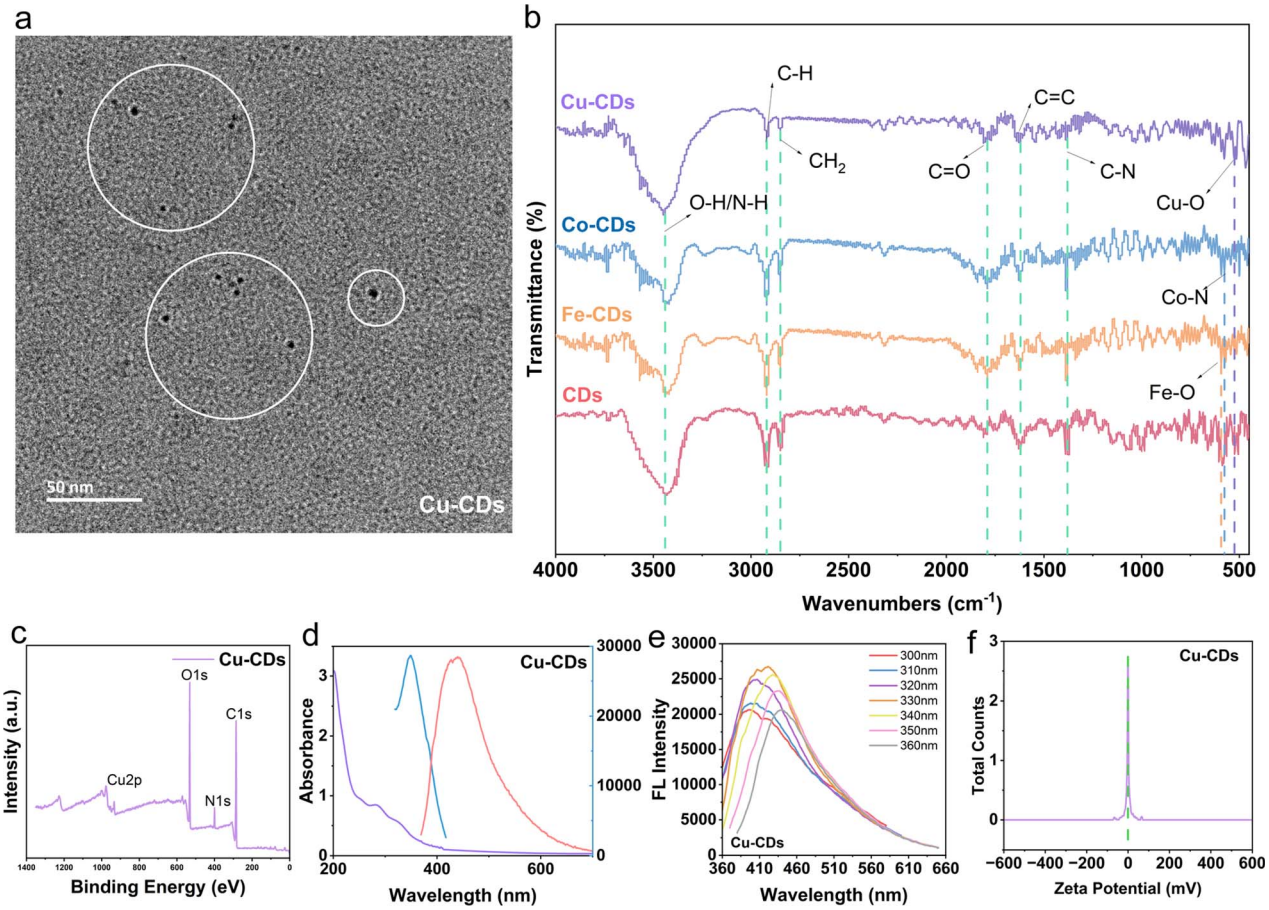

Fig. 1 Characterization of the CDs nanozymes. (a) TEM images of Cu-CDs. (b) FT-IR absorption spectra of all CDs. (c) XPS full spectrum. (d) UV-Vis absorption spectra, the emission spectra and the excitation spectra. (e) Fluorescence spectra under different excitation wavelength. (f) Zeta potential distribution of Cu-CDs.

elements into the CDs, thereby substantiating the preparation of Fe-CDs, Co-CDs, and Cu-CDs.

The optical properties of four types of CDs in deionized water were investigated using ultraviolet-visible (UV-Vis) absorption spectroscopy and fluorescence spectroscopy. The UV-Vis absorption spectra of Cu-CDs (Fig. 1d) and other three CDs (Fig. S4, ESI†) revealed a broad absorption band: the bands with peaks around 280 nm and 323 nm for the four types of CDs are likely attributed to the π–π* transitions within the C=C and n–π* transitions within C=O and bonds, associated with carbon core and the carbonyl functional groups.[48,49] All CDs demonstrated excellent fluorescence, with the optimal excitation and emission wavelengths for CDs being 345 and 445 nm, for Fe-CDs 340 and 435 nm, for Co-CDs 342 and 432 nm (Fig. S5, ESI†), and for Cu-CDs 418 and 330 nm (Fig. 1e).

Following the successful synthesis, we also tested the Zeta potentials of these CDs. Zeta potential is a key indicator that reflects the degree of repulsion between colloidal particles.[50] From the Zeta potential distribution graphs, we can observe that the Zeta potential peak values for these CDs, Fe-CDs and Co-CDs are at 1.96 mV, −0.856 mV, 2.78 mV (Fig. S6, ESI†), and for Cu-CDs is 3.11 mV (Fig. 1f), respectively. Notably, only Fe-CDs exhibited a slightly negative value, while Cu-CDs demonstrated the highest positive value and also had the better dispersion among the CDs with a larger absolute value.[51]

2.2 POD-like activity of the nanozymes

It has been reported that carbon-based nanoparticles possess effective POD-like activity, and these activities have been confirmed in applications such as cancer therapy and antibacterial treatments.[52,53] With the successful doping of Fe, Co, and Cu into CDs, we investigated the catalytic activities of these nanozymes. In the presence of H_2O_2 and a POD mimic, the colorless TMB is oxidized to a blue product, oxTMB. Nanozymes that can rapidly decompose H_2O_2, leading to a significant enhancement in the blue color of the reaction due to TMB oxidation, should exhibit extremely high reaction rates. When CDs were added to a solution containing only H_2O_2 at pH = 3.5, there is no noticeable change in color of the solution (Fig. 2a). The addition of Co-CDs, and Fe-CDs slightly increased the reaction rate, but not significantly, and the solution added Fe-CDs finally turned into light blue. However, upon the addition of Cu-CDs, there was a dramatic increase in the decomposition rate of the TMB substrate, and the solution turned a bright, deep blue, demonstrating that among the three synthesized metal-doped CDs, Cu-CDs most effectively catalyzed the

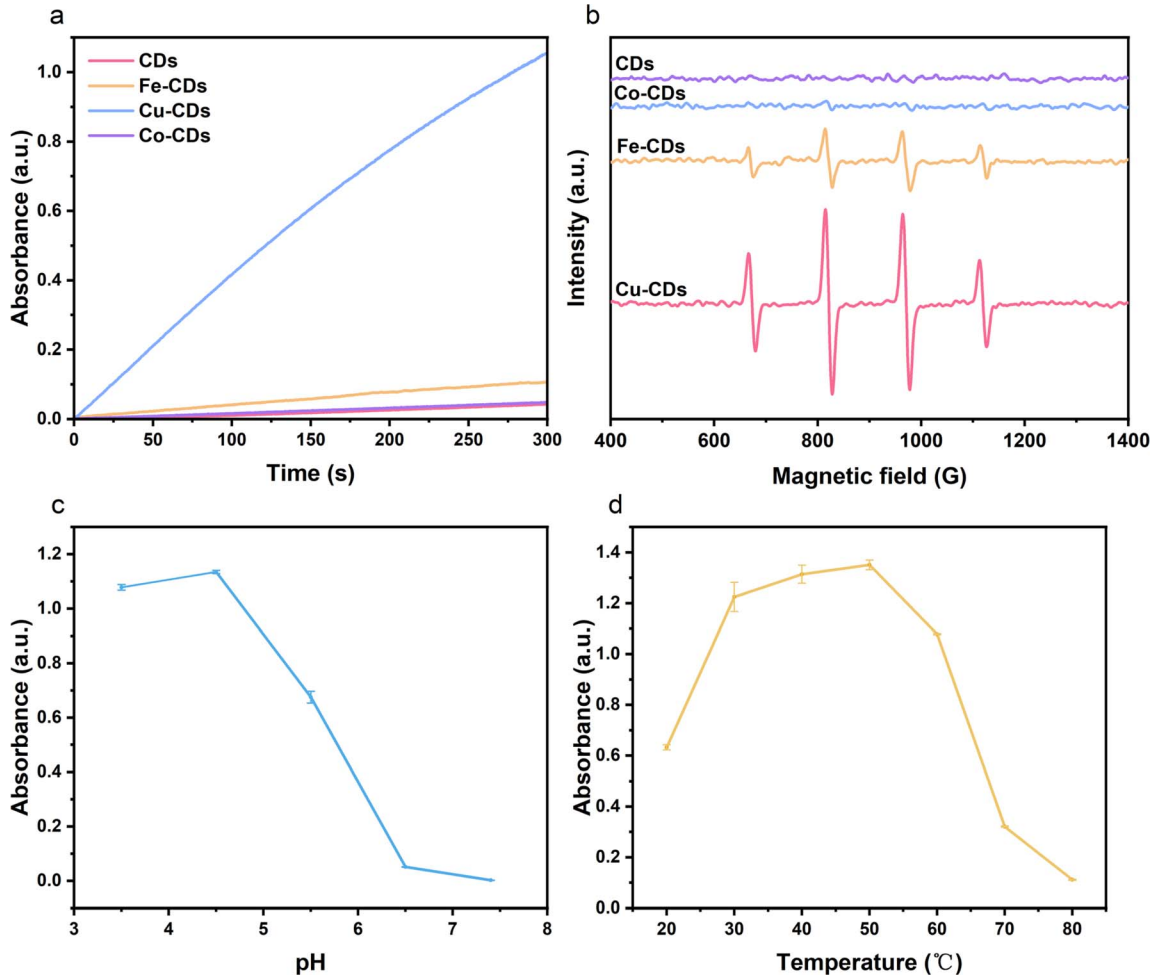

Fig. 2 Characterization of POD-like activity of CDs, Fe-CDs, Co-CDs and Cu-CDs. (a) UV-Vis absorption spectra of TMB solution oxidized by different CDs, accompanied by photograph of the solution. (b) ESR spectra of all CDs. (c) UV-Vis absorption spectra of TMB solution oxidized by Cu-CDs at various temperatures. (d) UV-Vis absorption spectra of TMB solution oxidized by Cu-CDs in PBS buffers at pH levels.

decomposition of H_2O_2. The substance decomposed by H_2O_2 is identified as the hydroxyl radical (·OH). We conducted electron spin resonance (ESR) tests on each type of CDs to detect the concentration of ·OH radicals produced by their catalysis in a solution of the same H_2O_2 concentration. Analysis of Fig. 2b reveals that CDs do not exhibit a pronounced detection peak. In comparison, Fe-CDs demonstrate a more distinct ·OH detection peak. In comparison, Fe-CDs demonstrate a more distinct ·OH detection peak. However, the detection peak for Cu-CDs is even more pronounced, indicating a higher concentration of ·OH produced.

In practice, the activity of natural enzymes depends on reaction parameters such as temperature and pH of the environment. Therefore, it is necessary to explore the impact of different reaction temperatures (20–80 °C) (Fig. 2c) and pH values (3.5–7.4) (Fig. 2d) on the activity of the most catalytically efficient Cu-CDs nanozymes. As the reaction temperature and pH increased, the nanozyme's activity generally followed a trend of initial increase followed by a decrease, with the graph indicating that the optimal reaction temperature for Cu-CDs nanozymes is around 50 °C, and the optimal pH is around 4.5.

2.3 Kinetic analysis of the nanozymes

Based on steady-state kinetics, we further investigated the catalytic performance of Cu-CDs nanoparticles. Kinetic data were obtained by keeping the concentration of one substrate constant while varying the concentration of TMB or H_2O_2 in the other substrate. The fitting of time and absorbance data produced a Michaelis–Menten curve, while the double reciprocal plot, known as the Lineweaver–Burk modification, of the Michaelis–Menten equation was utilized to calculate the kinetic parameters, which include the Michaelis constant (K_m) and the maximum initial reaction rate (V_{max}). V_{max} and K_m are important parameters for judging the level of POD-like activity.[54,55] When H_2O_2 is used as the substrate, the K_m value is 1.9138 mM, and the V_{max} is 7.0582×10^{-8} M s^{-1} (Fig. 3a and b). When TMB is used as the substrate, the K_m value is determined to be 0.65139 mM, and the V_{max} is 11.952×10^{-8} M s^{-1} (Fig. 3c and d).

2.4 Antibacterial activity of the nanozymes

Given the exceptional POD-like activity of Cu-CDs, we explored their application in antibacterial contexts. Using *E. coli* and *S. aureus* as representative bacterial strains, we evaluated the *in*

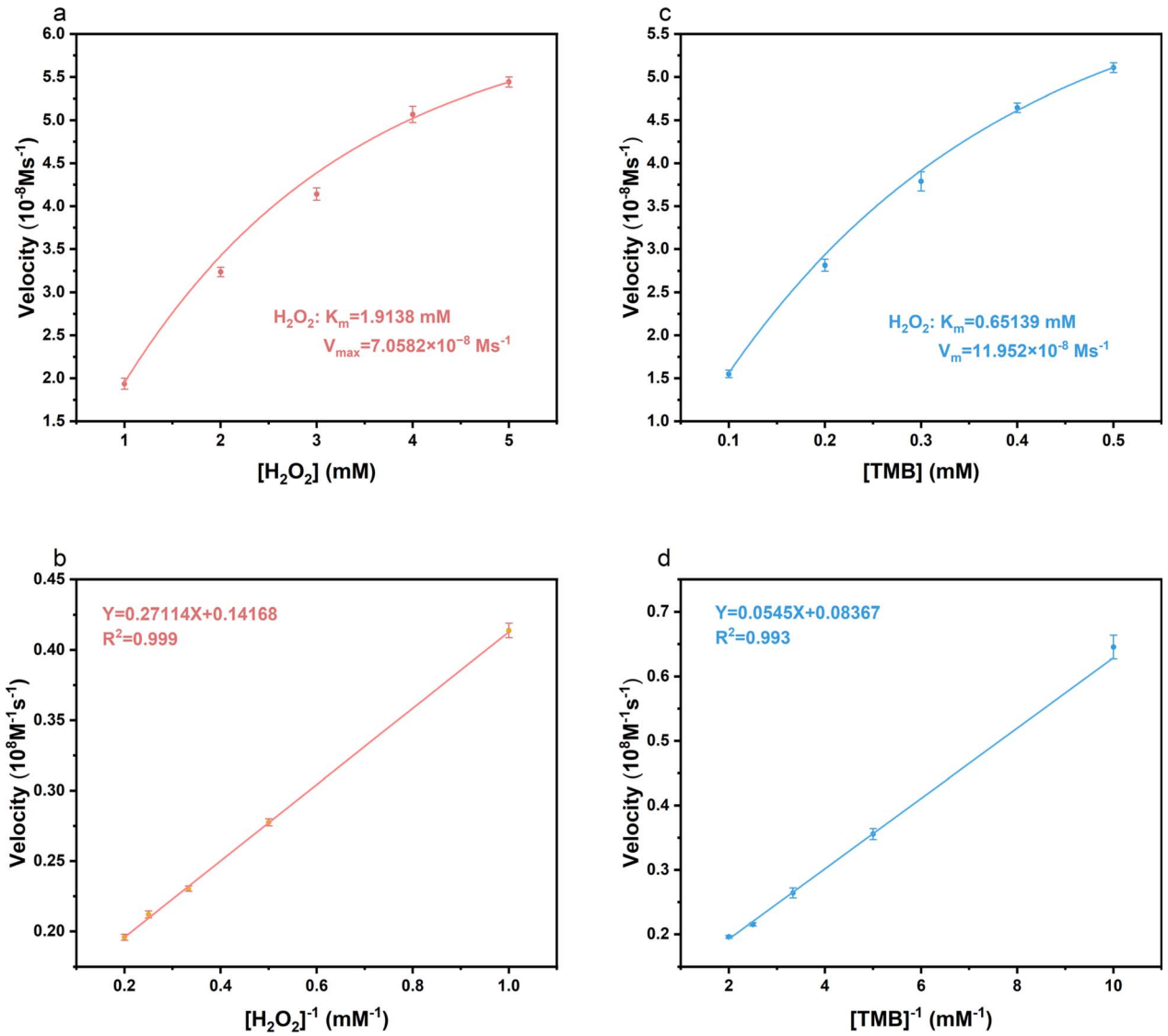

Fig. 3 Characterization of kinetic analysis of Cu-CDs. (a and b) Velocity of the solution at different H_2O_2 concentrations oxidized by Cu-CDs and the double-reciprocal plots of their activity. (c and d) Velocity of the solution at different TMB concentrations oxidized by Cu-CDs and the double-reciprocal plots of their activity.

vitro antibacterial effects of Cu-CDs nanozymes at the same concentration as the other three nanozymes using the plate count method.[56] We first only added the different concentration of H_2O_2 into *E. coli* to test the MIC of H_2O_2 (Fig. S7, ESI†). Initially, CDs were diluted into various gradient concentrations and added to bacterial solutions. As observed in the Fig. 3a, positively charged CDs at all concentrations showed slight toxicity to the bacteria (Fig. 4b and c). Subsequently, we selected a concentration of 500 μg mL^{-1} and mixed the four types of nanozymes with the bacterial solution before adding H_2O_2.

It is worth noting that the number of bacterial colonies in the control group without added H_2O_2 is comparable (Fig. S9, ESI†), while the group with added H_2O_2 containing nanozymes exhibit significant antibacterial effects (Fig. 4d), especially the plate containing Cu-CDs, where the number of bacterial colonies is markedly reduced.

When Cu-CDs are combined with H_2O_2, there is a noticeable decrease in relative bacterial viability, indicating that the nanozymes achieve antibacterial activity by generating hydroxyl radicals (·OH) through a Fenton-like reaction.[57–59] The significant reduction in the number of bacteria in the solution containing Cu-CDs is not only due to the positively charged Cu-CDs effectively capture negatively charged bacteria (Fig. S10, ESI†) through electrostatic interactions, but also because Cu-CDs exhibit higher catalytic activity like POD, which can trigger a Fenton-like reaction, thereby achieving efficient bactericidal activity. The antibacterial activity of the Cu-CDs is achieved through the synergistic effect of the activation of catalytic activity like POD triggered by the Fenton-like reaction and electrostatic interactions. Moreover, the antibacterial rates of Cu-CDs against bacteria are 90.76% and 91.53%, respectively (Fig. 4e and f). The MIC of Cu-CDs with H_2O_2 is also shown in Fig. S8, ESI.†

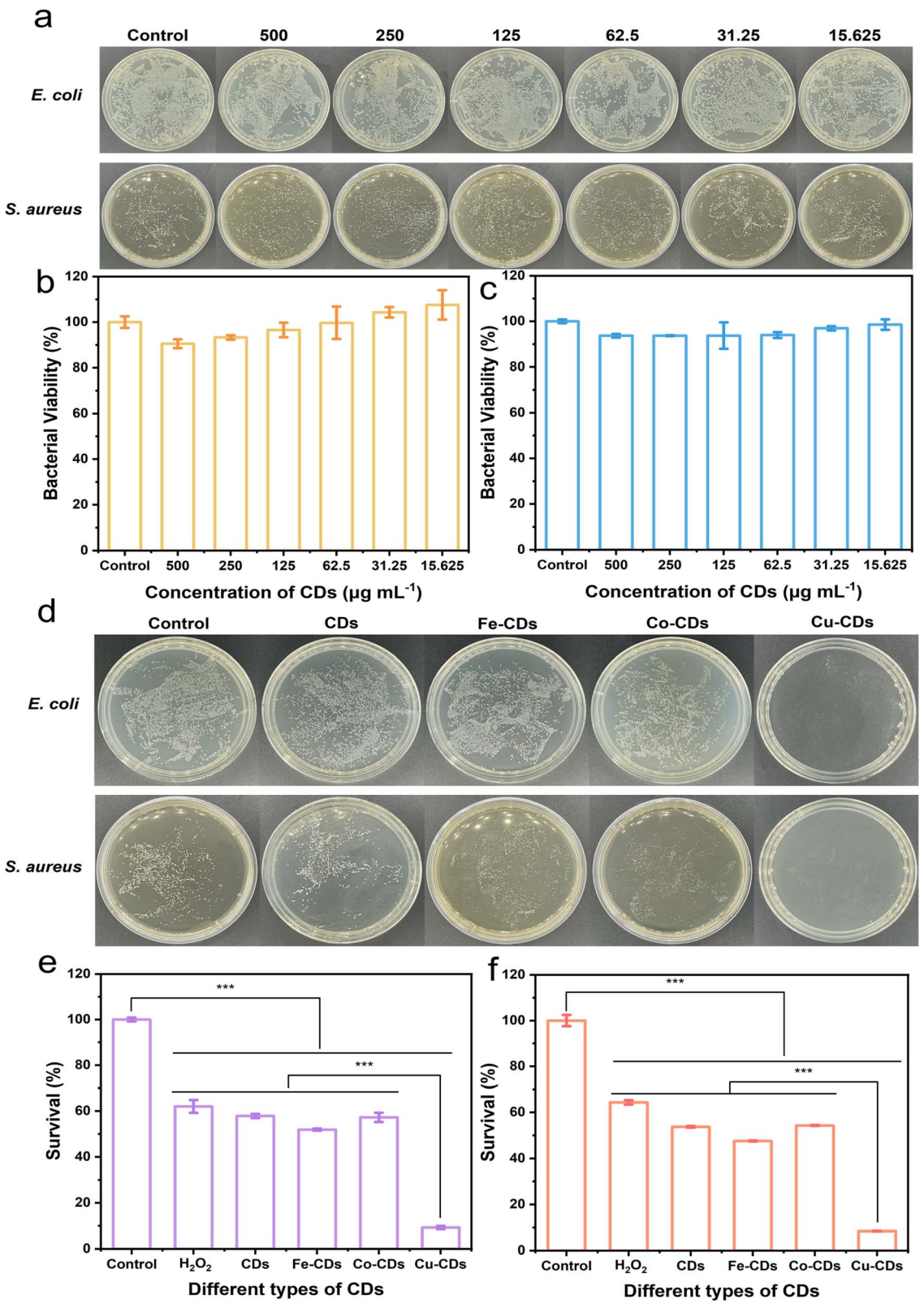

Fig. 4 Exploring antibacterial activity of CDs nanozymes. (a) Photograph of *E. coli* and *S. aureus* following exposure to CDs nanozymes at different concentrations. (b and c) Bacterial viability of *E. coli* and *S. aureus* following exposure to CDs nanozyme at different concentrations. (d) Photograph of *E. coli* and *S. aureus* treated with various CDs nanozymes with H_2O_2. (e and f) Survival rate of *E. coli* and S. *aureus* treated with various CDs nanozymes with H_2O_2. Data are presented as mean ± SD ($n = 3$), ns: $p > 0.05$, *$p < 0.05$, **$p < 0.01$, ***$p < 0.001$.

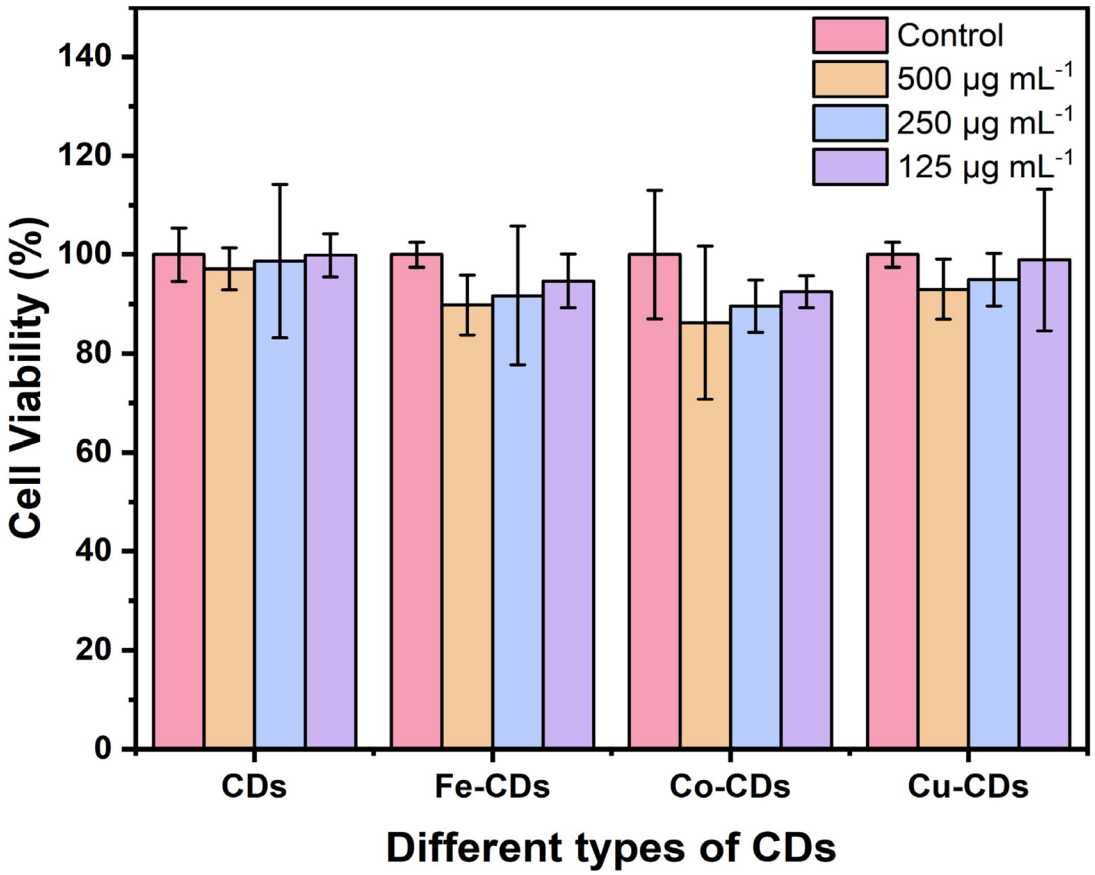

Fig. 5 Cell viability of all CDs at different final concentrations.

In comparison to the bacterial solution with only H_2O_2 added, the addition of Cu-CDs to the bacterial solution has led to a significant reduction in the counts of *E. coli* and *S. aureus*, dropping to 14.9% and 13.2% of the counts in the bacterial solution with only H_2O_2, respectively. This outcome underscores the remarkable antibacterial effects of Cu-CDs. These results indicate that the nanozymes we synthesized, especially the Cu-CDs nanozymes, are the most effective in inhibiting bacterial survival.

As a supplement, we conducted antibacterial circle experiments (Fig. S11, ESI†) on all CDs, and it can be observed that Cu-CDs still perform the best, with the relative antibacterial circle radius reaching 211.29% and 233.33% of the reference radius of 2.5 mm, respectively for *E. coli* and *S. aureus*, respectively.

These findings confirm the potential application of the Fenton-like reaction in the biological field and the ability of Cu-CDs to mimic and catalyze the oxidation of H_2O_2, providing a promising strategy for combating bacterial infections, especially against the backdrop of antibiotic.[60,61]

2.5 Cytotoxicity assay

Due to the necessity for antibacterial agents to possess low toxicity, minimizing the cytotoxicity of CDs is particularly crucial for their biological applications. Therefore, this experiment utilized L929 cells as a model and employed the CCK-8 assay to evaluate the *in vitro* cytotoxicity of four types of CDs. The results are depicted in the figure. Overall, there was a slight decrease in the cell viability (Fig. 5) of L929 cells as the concentration of CDs increased. The findings indicate that when the final concentration reached 500 μg mL^{-1}, the cell viability after a 24 hour incubation with all CDs remained above 85%, with the Cu-CDs showing particularly promising results, exceeding 90% cell viability.

To further investigate the cytotoxicity of CDs on human cells, we conducted cytotoxicity tests on human skin fibroblasts (HSF) using the highest concentration of 500 μg mL^{-1} (Fig. S12, ESI†), which was also applied to L929 mouse cells under the same conditions. Among the tested CDs, Co-CDs exhibited the lowest cell viability at 85.99%; however, the cell viability of all CDs exceeded 85%, indicating a low toxicity level towards human cells. These outcomes suggest that CDs exhibit good biosafety profiles.

3. Conclusions

In this study, we successfully synthesized a series of cherry blossom CDs doped with various metals and comprehensively evaluated their POD-like enzymatic activity and kinetic parameters. Through in-depth analysis of these nanozymes, we observed that Cu-CDs demonstrated significant advantages in mimicking the activity of natural PODs, with catalytic efficiency and stability that surpassed other metal-doped CDs. The exceptional performance of Cu-CDs positions them for better applications in

multiple medical fields, including antibacterial disinfection, biosensing, and disease treatment. During the development of antimicrobial agents, a critical consideration is how to minimize potential harm to normal healthy cells. To assess the safety and biocompatibility of these CDs, we conducted cytotoxicity tests. The experimental results indicated that even at higher concentrations, Cu-CDs, along with the other three types of CDs, maintained low toxicity to cells, which is particularly important for their application as clinical therapeutic agents.

In previous studies, we have also frequently observed examples of enhancing POD-like activity in nanomaterials by doping with copper.[38,47,62–65] This study similarly found that Cu-CDs performed optimally, which not only confirms the important role of copper in enhancing the enzymatic activity of CDs but also provides a solid experimental basis for future applications in biosensing, disease diagnosis, and antimicrobial treatment. We believe that Cu-CDs, as an efficient and safe nanozyme, not only offer new solutions for antimicrobial therapy but also hold promise for playing a significant role in other biomedical fields. With a deeper understanding of the structure–function relationship of Cu-CDs, they are expected to play an even more important role in precision medicine.

4. Materials and methods

4.1 Chemicals

The cherry blossoms were handpicked from Shanghai University, ensuring the authenticity and quality of our botanical samples. Iron(III) chloride hexahydrate ($FeCl_3 \cdot 6H_2O$) was sourced directly from SIGMA-ALDRICH Co., Ltd. A selection of other reagents, including 3,3′,5,5′-tetramethyl benzidine (TMB), cobalt chloride hexahydrate ($CoCl_2 \cdot 6H_2O$), and cupric chloride dihydrate ($CuCl_2 \cdot 2H_2O$), were acquired from Aladdin Chemistry Reagent Co., Ltd. The cultivation media, Luria broth (LB), agar powder and tryptone soy broth (TSB) were provided by Solarbio Science & Technology Co., Ltd. Fetal bovine serum (FBS), Dulbecco's modified Eagle's medium (DMEM), and the antibiotic mixture penicillin/streptomycin (PS) were all sourced from Sangon Biotech Co., Ltd. Phosphate-buffered saline (PBS) was purchased from Leagene Biotechnology Co., Ltd. To ensure the utmost purity and precision in our experimental procedures, all solutions were prepared using ultrapure water with a resistivity of 18.2 MΩ cm from the Milli-Q system.

4.2 Instruments

The samples were subjected to physical characterization using a Transmission Electron Microscope (TEM) (FEI Company, United States), model Tecnai G2 F20 S-Twin TMP. Optical density measurements were conducted using an Ultraviolet-Visible (UV-Vis) Spectrophotometer (PerkinElmer, United States), specifically the Lambda 750 model. To assess the fluorescence properties of the samples, we employed the FS5 Spectrofluorometer (Edinburgh Instruments, United Kingdom). X-ray Photoelectron Spectroscopy (XPS) analyses were performed on the Kratos Axis Ultra DLD (KRATOS, United Kingdom). Furthermore, Fourier-Transform Infrared (FT-IR) spectroscopic analysis was carried out using the Nicolet iS50 FT-IR Spectrometer (Thermo Fisher Scientific, United States) and zeta potential measurements were conducted using the Liteser 500 (Anton Paar, Austria). The analysis of electron spin resonance (ESR) was conducted utilizing a Bruker EMX ESR spectrometer (Bruker, Germany).

4.3 Synthesis of the CDs

All CDs were synthesized *via* the one-step hydrothermal method. Initially, the collected cherry blossom petals were placed in an oven and dried at 60 °C for 48 hours. After being thoroughly dried, the petals were crushed into a delicate powder using a grinding apparatus. Next, a measurement of 0.5 g was taken from the powdered cherry blossoms (for the creation of metal-doped CDs, supplementary amounts of 0.08 g $FeCl_3 \cdot 6H_2O$, 0.0843 g $CoCl_2 \cdot 6H_2O$, or 0.0914 g $CuCl_2 \cdot 2H_2O$ were mixed in) to this and 20 mL of a half-strength ethanol solution were added. After mixing, the mixture was sonicated for 20 minutes and then transferred to a 50 mL Teflon-lined hydrothermal reactor, where it was subjected to heating at 180 °C for 8 hours. The resulting solution was de-ethanolized using a rotary evaporator, and the obtained brown solution was filtered through a 0.22 μm microfiltration membrane. The solution was then dialyzed using a 1000 Da dialysis membrane for three days. The fractions that exhibited bright blue fluorescence under ultraviolet light were obtained, thus completing the synthesis of a solution containing cherry blossom-derived CDs.

4.4 POD-like activity

The colorimetric substrate 3,3′,5,5′-tetramethylbenzidine (TMB) was oxidized in Phosphate Buffered Saline (PBS) buffer solution containing CDs doped with various metals, with a working final concentration of H_2O_2 at 5 mmol L^{-1}, TMB at 0.5 mmol L^{-1}, and CDs at 50 μg mL^{-1}. Firstly, the experiment was conducted at room temperature (20 °C) in a PBS buffer solution with a pH of 3.5 to identify the metal-doped CDs with the strongest POD-like activity. Subsequently, Cu-CDs, which demonstrated the highest POD-like activity, were dissolved in PBS buffer solutions at other different pH levels (pH 4.5, 5.5, 6.5, 7.4), maintaining consistent working final concentrations for H_2O_2, TMB, and CDs, as well as the temperature, to determine the pH at which Cu-CDs exhibit the quickest catalytic rate. Finally, the pH condition with the best POD-like activity (pH = 4.5) was selected, and CDs were dissolved in the corresponding pH PBS buffer. The concentrations of H_2O_2, TMB, and CDs were kept as before, and the reaction rates were tested at various temperatures (20, 30, 40, 50, 60, 70, 80 °C) to obtain the best temperature (50 °C). In addition to this, we also conducted Electron Spin Resonance (ESR) tests on four types of CDs.

4.5 Enzyme kinetics studies

At the best working temperature of 50 °C, samples were dissolved in PBS buffer solution (pH = 4.5) and prepared into solutions with varying concentrations of H_2O_2 (final working concentrations: 1, 2, 3, 4, 5 mmol L^{-1}) and TMB (final working concentrations: 0.1, 0.2, 0.3, 0.4, 0.5 mmol L^{-1}). The final

working concentration of Cu-CDs was set at 50 μg mL^{-1}, and the enzyme-catalyzed reaction rates were measured. The final working concentration of TMB, used for H_2O_2 kinetics determination, was 0.5 mmol L^{-1}, while the final working concentration of H_2O_2, used for TMB kinetics determination, was 5 mmol L^{-1}. The kinetics of the process were calculated using the Michaelis–Menten eqn (1), where K_m represents the Michaelis–Menten constant, V denotes the initial reaction velocity, V_{max} signifies the maximum reaction rate, and C indicates the substrate concentration:[66]

$$\frac{1}{V} = \frac{K_m}{CV_{max}} + V_{max} \quad (1)$$

4.6 Antibacterial testing

Specific bacterial strains, such as *E. coli*, were cultured in Luria-Bertani (LB) broth, and *S. aureus* were cultured in soybean-meat broth. Subsequently, bacterial cultures were diluted to a specific concentration (OD_{600} = 0.1, corresponding to 10^8 CFU mL^{-1}). These bacterial solutions were divided into different groups, each first co-cultured with CDs nanozyme at various final concentrations (500, 250, 125, 62.5, 31.25, 15.625 μg mL^{-1}), followed by co-cultivation with Fe-CDs, Co-CDs, and Cu-CDs solutions at a concentration of 250 μg mL^{-1}. These results demonstrate that CDs do not exhibit particular toxicity towards bacteria. Subsequently, by mixing CDs with a 10^{-3} M H_2O_2 solution and co-cultivating them with bacteria, it was shown that the antibacterial activity of Cu-CDs is superior to that of other CDs. The incubation period was set for 12 hours at a temperature of 37 °C, after which the absorbance was measured using a microplate reader at a wavelength of 600 nm.

4.7 Cytotoxicity assay

In this study, we evaluated the cytotoxicity of all CDs on L929 mouse fibroblast cells and Human Skin Fibroblast (HSF) cells using the CCK-8 colorimetric assay.[67] All the CDs were introduced into the L929 cell culture to achieve final concentrations of 500, 250, 125 μg mL^{-1}. For HSF cells, we utilized the maximum concentration of 500 μg mL^{-1} for our assessment. After a 24 hour incubation period, 10 μl CCK-8 solution was added to each well. Following a further 4 hour incubation, then the absorbance was measured at 450 nm using a microplate reader.

Data availability

All data that support the findings of this study are included in this manuscript and its ESI files.†

Conflicts of interest

There are no conflicts to declare.

Acknowledgements

This work was funded by the National Natural Science Foundation of China [No. 22122704 and No. 22177067]; the Program for Distinguished Professor of Shanghai Universities (Oriental Scholars), Tracking Plan GZ202209.

References

1 M. Kolpen, K. N. Kragh, J. B. Enciso, D. Faurholt-Jepsen, B. Lindegaard, G. B. Egelund, A. V. Jensen, P. Ravn, I. H. M. Mathiesen, A. G. Gheorge, F. B. Hertz, T. Qvist, M. Whiteley, P. Ø. Jensen and T. Bjarnsholt, *Thorax*, 2022, **77**, 1015–1022.
2 M. Aires-de-Sousa, *Clin. Microbiol. Infect.*, 2017, **23**, 373–380.
3 M. Stracy, O. Snitser, I. Yelin, Y. Amer, M. Parizade, R. Katz, G. Rimler, T. Wolf, E. Herzel, G. Koren, J. Kuint, B. Foxman, G. Chodick, V. Shalev and R. Kishony, *Science*, 2022, **375**, 889–894.
4 D. Ashiru-Oredope, M. Nabiryo, E. M. Krockow and S. Essack, *Lancet*, 2022, **399**, 2348–2349.
5 M. I. Hutchings, A. W. Truman and B. Wilkinson, *Curr. Opin. Microbiol.*, 2019, **51**, 72–80.
6 R. Zhang, X. Yan and K. Fan, *Acc. Mater. Res.*, 2021, **2**, 534–547.
7 Z. Wang, R. Zhang, X. Yan and K. Fan, *Mater. Today*, 2020, **41**, 81–119.
8 X. Wang, H. Wang and S. Zhou, *J. Phys. Chem. Lett.*, 2021, **12**, 11751–11760.
9 A. Biby, H. Crawford and X. Xia, *ACS Appl. Nano Mater.*, 2022, **5**, 17622–17631.
10 B. Yuan, H.-L. Chou and Y.-K. Peng, *ACS Appl. Mater. Interfaces*, 2022, **14**, 22728–22736.
11 X. Wang, Q. Shi, Z. Zha, D. Zhu, L. Zheng, L. Shi, X. Wei, L. Lian, K. Wu and L. Cheng, *Bioact. Mater.*, 2021, **6**, 4389–4401.
12 G. Yim, C. Y. Kim, S. Kang, D.-H. Min, K. Kang and H. Jang, *ACS Appl. Mater. Interfaces*, 2020, **12**, 41062–41070.
13 M. G. Giordano, G. Seganti, M. Bartoli and A. Tagliaferro, *Molecules*, 2023, **28**, 2772.
14 M. Li, T. Chen, J. J. Gooding and J. Liu, *ACS Sens.*, 2019, **4**, 1732–1748.
15 T. C. Wareing, P. Gentile and A. N. Phan, *ACS Nano*, 2021, **15**, 15471–15501.
16 S. Li, L. Li, H. Tu, H. Zhang, D. S. Silvester, C. E. Banks, G. Zou, H. Hou and X. Ji, *Mater. Today*, 2021, **51**, 188–207.
17 L. Đorđević, F. Arcudi, M. Cacioppo and M. Prato, *Nat. Nanotechnol.*, 2022, **17**, 112–130.
18 K. O. Boakye-Yiadom, S. Kesse, Y. Opoku-Damoah, M. S. Filli, M. Aquib, M. M. B. Joelle, M. A. Farooq, R. Mavlyanova, F. Raza, R. Bavi and B. Wang, *Int. J. Pharm.*, 2019, **564**, 308–317.
19 S. Y. Lim, W. Shen and Z. Gao, *Chem. Soc. Rev.*, 2015, **44**, 362–381.
20 N. Baig, I. Kammakakam and W. Falath, *Mater. Adv.*, 2021, **2**, 1821–1871.
21 P. Du, Z. Chu, J. Zhang, J. Ma, F. Cao and J. Liu, *Biomass Conv. Bioref.*, 2023, DOI: 10.1007/s13399-023-04036-9.
22 Y. Zhu, X. Deng, J. Chen, Z. Hu and F. Wu, *Food Chem.*, 2023, **429**, 136957.
23 Y. Masago and M. Lian, *Ecol. Inf.*, 2022, **71**, 101835.

24 M. Strzałkowska-Abramek, *Folia Horticulturae*, 2019, **31**, 205–212.
25 Q. Xiang, S. Sun, Y. Liu, Z. Wu and X. Zhang, *Food Biosci.*, 2023, **55**, 103051.
26 J. Lee, G. Yang, K. Lee, M.-H. Lee, J.-W. Eom, I. Ham and H.-Y. Choi, *BMC Complement. Altern. Med.*, 2013, **13**, 92.
27 Y. Q. Zhang, L. Guan, Z. Y. Zhong, M. Chang, D. K. Zhang, H. Li and W. Lai, *Int. J. Cosmet. Sci.*, 2014, **36**, 527–530.
28 K. Huang, Q. He, R. Sun, L. Fang, H. Song, L. Li, Z. Li, Y. Tian, H. Cui and J. Zhang, *Chem. Phys. Lett.*, 2019, **731**, 136586.
29 J. Dong, G. Liu, Y. V. Petrov, Y. Feng, D. Jia, V. E. Baulin, A. Y. Tsivadze, Y. Zhou and B. Li, *ACS Mater. Lett.*, 2024, **6**, 1112–1119.
30 Z. Yang, Y. Liu, C. Lu, G. Yue, Y. Wang, H. Rao, W. Zhang, Z. Lu and X. Wang, *J. Alloys Compd.*, 2021, **862**, 158323.
31 Y. Shen, R. Zhang and Y. Wang, *RSC Adv.*, 2023, **13**, 6760–6767.
32 X. Ren, D. Chen, Y. Wang, H. Li, Y. Zhang, H. Chen, X. Li and M. Huo, *J. Nanobiotechnol.*, 2022, **20**, 92.
33 Y. Guo, Z. Wang, Y. Chen, F. Chao, Y. Xu, L.-L. Qu, F.-G. Wu and X. Dong, *Nano Lett.*, 2024, **24**, 2264–2272.
34 F. Gao, J. Liu, P. Gong, Y. Yang and Y. Jiang, *Chem. Eng. J.*, 2023, **462**, 142338.
35 J. Liu, F. Gao, L. Zhao, Y. Wu, F. Wang, L. Dong and Y. Jiang, *Ceram. Int.*, 2023, **49**, 25253–25260.
36 X. Li, H. Zhu, P. Liu, M. Wang, J. Pan, F. Qiu, L. Ni and X. Niu, *Trac. Trends Anal. Chem.*, 2021, **143**, 116379.
37 B. Yan, Y. Yang, Y. Xie, J. Li and K. Li, *Chemistry*, 2023, **5**, 1302–1316.
38 Y. Wang, J. Yao, Z. Cao, P. Fu, C. Deng, S. Yan, S. Shi and J. Zheng, *Chem. –Eur. J.*, 2022, **28**, e202104174.
39 Y. Wang, H. Li, L. Guo, Q. Jiang and F. Liu, *RSC Adv.*, 2019, **9**, 18815–18822.
40 W. Lu, Y. Guo, J. Zhang, Y. Yue, L. Fan, F. Li, C. Dong and S. Shuang, *ACS Appl. Mater. Interfaces*, 2022, **14**, 57206–57214.
41 J. Wu, X. Wang, Q. Wang, Z. Lou, S. Li, Y. Zhu, L. Qin and H. Wei, *Chem. Soc. Rev.*, 2019, **48**, 1004–1076.
42 C. Liu, M. Zhang, H. Geng, P. Zhang, Z. Zheng, Y. Zhou and W. He, *Appl. Catal. B Environ.*, 2021, **295**, 120317.
43 F. Cui, L. Li, D. Wang, L. Ren, J. Li, Y. Lu, Y. Meng, R. Ma, S. Wang, X. Li, T. Li and J. Li, *Chem. Eng. J.*, 2023, **473**, 145291.
44 F. Lin, Y.-W. Bao and F.-G. Wu, *C*, 2019, **5**, 33.
45 Q. Ci, Y. Wang, B. Wu, E. Coy, J. J. Li, D. Jiang, P. Zhang and G. Wang, *Adv.Sci.*, 2023, **10**, 2206271.
46 L. Lin, Y. Xiao, Y. Wang, Y. Zeng, Z. Lin and X. Chen, *Microchim. Acta*, 2019, **186**, 288.
47 Q. Li, D. Yang and Y. Yang, *Spectrochim. Acta Mol. Biomol. Spectrosc.*, 2021, **244**, 118882.
48 J. Zhang, Y. Lin, S. Wu, X. Hou, C. Zheng, P. Wu and J. Liu, *Carbon*, 2021, **182**, 537–544.
49 J.-C. Kung, I.-T. Tseng, C.-S. Chien, S.-H. Lin, C.-C. Wang and C.-J. Shih, *RSC Adv.*, 2020, **10**, 41202–41208.
50 D. Zhu, M. Zhang, L. Pu, P. Gai and F. Li, *Small*, 2022, **18**, 2104993.
51 T. Wang, Y. Sun, L. Zhang, K. Li, Y. Yi, S. Song, M. Li, Z. Qiao and S. Dai, *Adv. Mater.*, 2019, **31**, 1807876.
52 J. Liu, R. Li and B. Yang, *ACS Cent. Sci.*, 2020, **6**, 2179–2195.
53 J. Dong, G. Liu, Y. V. Petrov, Y. Feng, D. Jia, V. E. Baulin, A. Y. Tsivadze, Y. Zhou and B. Li, *ACS Mater. Lett.*, 2024, **6**, 1112–1119.
54 M. Liang, Y. Wang, K. Ma, S. Yu, Y. Chen, Z. Deng, Y. Liu and F. Wang, *Small*, 2020, **16**, 2002348.
55 C. Park, *J. Chem. Educ.*, 2022, **99**, 2556–2562.
56 T. Wang, Q. Bai, Z. Zhu, H. Xiao, F. Jiang, F. Du, W. W. Yu, M. Liu and N. Sui, *Chem. Eng. J.*, 2021, **413**, 127537.
57 J. Lin, W. Tian, Z. Guan, H. Zhang, X. Duan, H. Wang, H. Sun, Y. Fang, Y. Huang and S. Wang, *Adv. Funct. Mater.*, 2022, **32**, 2201743.
58 B. Ma, S. Wang, F. Liu, S. Zhang, J. Duan, Z. Li, Y. Kong, Y. Sang, H. Liu, W. Bu and L. Li, *J. Am. Chem. Soc.*, 2019, **141**, 849–857.
59 J. Huang, F. Gao, Q. Liu, P. Gong, H. Li and Y. Jiang, *Small*, 2024, **20**, 2309637.
60 T. Li, L. Lin, D. Wang, H. Fang, Z. Zhang, Y. Wang, Y. Chen and L. Feng, *Adv. Therap*, 2024, 2300368.
61 S. Zhang, Z. Yang, J. Hao, F. Ding, Z. Li and X. Ren, *Chem. Eng. J.*, 2022, **432**, 134309.
62 F. Gao, J. Huang, Y. Ruan, H. Li, P. Gong, F. Wang, Q. Tang and Y. Jiang, *Angew. Chem., Int. Ed.*, 2023, **62**, e202214042.
63 Z. Gu, D. Zhong, X. Hou, X. Wei, C. Liu, Y. Zhang, Z. Duan, Z. Gu, Q. Gong and K. Luo, *Adv. Sci.*, 2024, **11**, 2307154.
64 Q. Li, D. Yang, Q. Yin, W. Li and Y. Yang, *ACS Appl. Nano Mater.*, 2022, **5**, 1925–1934.
65 M. Liu, L. Huang, X. Xu, X. Wei, X. Yang, X. Li, B. Wang, Y. Xu, L. Li and Z. Yang, *ACS Nano*, 2022, **16**, 9479–9497.
66 S. Chakraborty, S. Kolay, S. Maity and A. Patra, *Langmuir*, 2024, **40**, 317–324.
67 P. Liu, Y. Feng, H. Li, X. Chen, G. Wang, S. Xu, Y. Li and L. Zhao, *Cell. Mol. Biol. Lett.*, 2020, **25**, 10.